Two-dimensional skyrmion bags in liquid crystals and ferromagnets

David Foster,[1] Charles Kind,[2] Paul J. Ackerman,[3] Jung-Shen B. Tai,[3] Mark R. Dennis,[1,4] and Ivan I. Smalyukh[3,5,6]

[1]*H. H. Wills Physics Laboratory, University of Bristol, Bristol BS8 1TL, UK*
[2]*School of Mathematics, University of Bristol, Bristol BS8 1TW, UK*
[3]*Department of Physics and Soft Materials Research Center, University of Colorado, Boulder, Colorado 80309, USA*
[4]*School of Physics and Astronomy, University of Birmingham, Birmingham B15 2TT, UK*
[5]*Department of Electrical, Computer, and Energy Engineering, Materials Science and Engineering Program, University of Colorado, Boulder, Colorado 80309, USA*
[6]*Renewable and Sustainable Energy Institute, National Renewable Energy Laboratory and University of Colorado, Boulder, Colorado 80309, USA*

(Dated: February 6, 2019)

Reconfigurable, ordered matter offers great potential for future low-power computer memory by storing information in energetically stable configurations. Among these, skyrmions – which are topologically protected, robust excitations, have been demonstrated in chiral magnets [1–4] and in liquid crystals [5–7] – are driving much excitement about potential spintronic applications [8]. These information encoding structures topologically resemble field configurations in many other branches of physics and have a rich history [9], although chiral condensed matter systems so far have only yielded realisations of elementary full and fractional skyrmions. Here we describe stable, high degree multi-skyrmion configurations where an arbitrary number of anti-skyrmions are contained within a larger skyrmion. We call these structures skyrmion bags. We demonstrate them experimentally and numerically in liquid crystals and numerically in micromagnetic simulations either without or with magnetostatic effects. We find that skyrmion bags act like single skyrmions in pairwise interaction and under the influence of current in magnetic materials, and are thus an exciting proposition for topological magnetic storage and logic devices.

Skyrmions are particle-like topological excitations studied in many condensed matter systems. For example, some of the earliest reports of liquid crystals (LCs) in the 1800s dealt with chiral phases in cholesterol derivatives extracted from animals, including the so-called 'blue phase' [10–12]. Decades later, these phases were demonstrated to be arrays of fractional skyrmions (also called 'merons'), cubic and hexagonal lattices of double-twist tubes in molecular alignment described by the director field $\boldsymbol{n}(\boldsymbol{x})$ with nonpolar head-tail symmetry [7, 12]. The rod-like molecules in such a tube are arranged to be parallel to its axis at its center, twisting radially outwards to form barber-pole-like patterns on concentric cylindrical surfaces (Fig. 1**a-c**). Elementary full LC skyrmion tubes, with such a 180° radial twist from center to periphery [5, 6], exhibit all possible molecular orientations, can be embedded in a uniform far-field background and enjoy topological protection (Fig. 1**d,i** & Supplementary Information Fig. **S1**). In a simply connected manifold, a smooth director structure can always be vectorized and gives a smooth vector configuration (compare Fig. 1**c,d** with Fig. 1**h,i**), a process in which the order parameter space changes from $\mathbb{S}^2/\mathbb{Z}_2$ to $\mathbb{S}^2$ (Fig. 1**b,g**). Therefore, a large number of topologically equivalent solitonic structures have been observed and exhibit similar behaviour in LCs and other condensed matter systems, such as magnets. The vectorized field can be in two antiparallel orientations and be given topological degrees Q with opposite signs [13]. Here we adopt the convention $Q = -1$ for an elementary full skyrmion in Fig. 1**d** [14].

The discovery of similar skyrmion configurations in the magnetization field in chiral magnets drives much excitement in spintronics [8]: magnetic skyrmions can be accelerated with a current [15, 16], so they might be used to encode data in racetrack memory technology [16–19]. The density of such information could be increased using skyrmions with varying topological degrees (whose distinction is topologically protected). One could consider realising high-degree skyrmions by introducing an extra π-twist beyond the fundamental full skyrmion, equivalent to placing a skyrmion inside another skyrmion (Fig. 1**j**). However, this coaxial structure, so-called skyrmionium, has zero topological charge. The process of placing central (anti)skyrmions inside a larger skyrmion, while maintaining axial symmetry, can be iterated to produce configurations with multiple π-twists from centre to far-field periphery, called target skyrmions (Fig. 2**a**). The topological degree of such axial configurations, increasing layers of π-twists, alternates between 0 and -1 due to cancellation from the contribution of adjacent twists, and therefore the inventory of topological degree is not extended. Only fractional and elementary full skyrmions have previously been realised in chiral condensed matter systems.

In this letter we report the discovery of stable chiral composite *skyrmion bags* which can have arbitrary topological

degree. We experimentally realise and numerically study them in LCs and in models and micromagnetic simulations of ferromagnets, demonstrating their enhanced stability, in the latter case both without and with the influence of demagnetising field effects. Using a combination of laser tweezers and videomicroscopy we experimentally probe pair interaction between skyrmions and skyrmion bags in LCs and demonstrate how their behaviour resembles that in the magnetic counterparts. These high-degree skyrmion configurations may enable a new paradigm-changing approach in encoding information in magnetic data storage, as well as could lead to electro-optic, microfluidic, nanoparticle transport and display applications dealing with topologically protected multi-stable states of chiral LC matter.

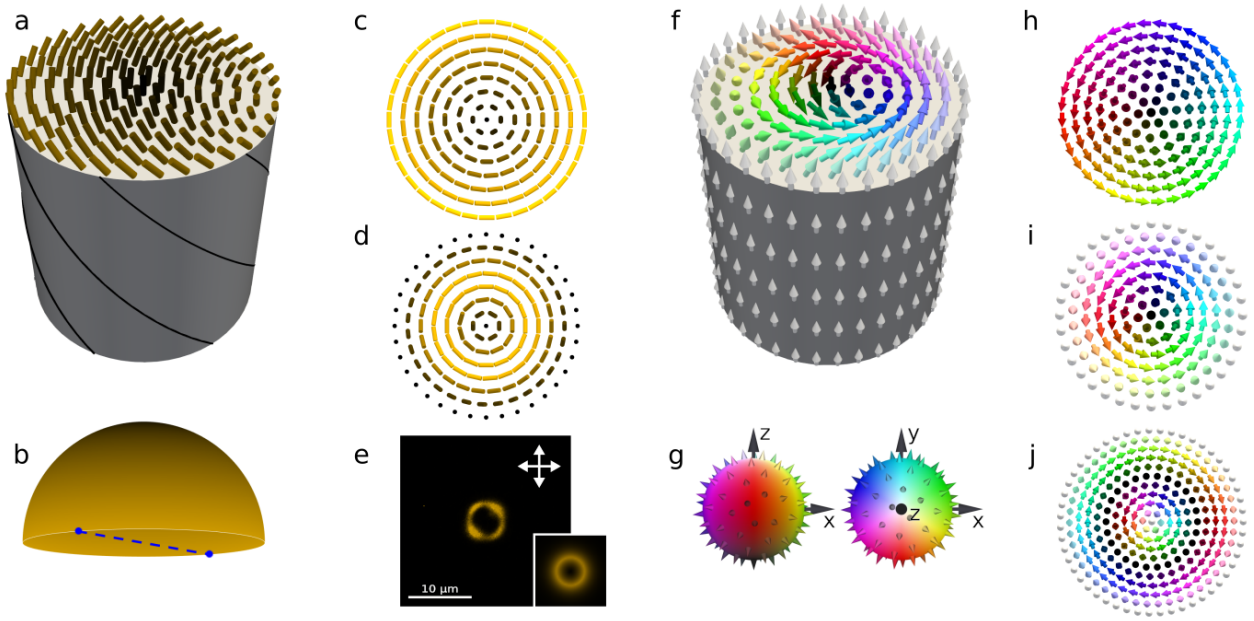

Figure 1: **Solitonic structures of a fractional skyrmion, skyrmion and skyrmionium (a)** A translationally invariant quarter-skyrmion tube with $\boldsymbol{n}(\boldsymbol{x})$, visualized by rods whose colour is based on their orientations in the $\mathbb{S}^2/\mathbb{Z}_2$ order-parameter space shown in **(b)**. **(b)** The colour scheme for $\boldsymbol{n}(\boldsymbol{x})$ in **(a-e)** determined by orientations in $\mathbb{S}^2/\mathbb{Z}_2$, where diametrically opposite points around the base of hemisphere are identified. **(c,d)** Top views of a half-skyrmion and an elementary full skyrmion in the director field, respectively. **(e)** A polarising optical micrograph of a LC skyrmion. The computer visualisation based on the colour scheme in **(b)** is shown in the inset. **(f)** A translationally invariant skyrmion tube visualized by coloured arrows smoothly decorating $\boldsymbol{n}(\boldsymbol{x})$ based on their orientations on the $\mathbb{S}^2$ sphere in **(g)**. **(g)** The Runge colour sphere is used for the vectors in **(f-j)**, with hues and brightness determined by the representation of $\boldsymbol{n}(\boldsymbol{x})$ on $\mathbb{S}^2$, viewing from the side and from above. **(h-j)** Top views of a vector-field half-skyrmion, full skyrmion, and skyrmionium, respectively.

In LCs, multiple π-twist target skyrmions can be generated by iterating the process of stretching a skyrmion with laser tweezers, then creating an antiskyrmion inside. We have found these configurations to have poor stability and existing only as transient structures. For example, a 6π-twist LC target skyrmion collapsing within 3 minutes is illustrated in Fig. 2**a** and in Video **S1**. The equivalence of the field topology of target skyrmions to an elementary full skyrmion (with odd number of π twists) or the uniform state (with even number of π twists) is also demonstrated in supplementary Video **S2**, where a 2π-twist skyrmionium transforms smoothly to the uniform trivial state.

Unlike the composite skyrmions that occur in the Skyrme model [9], elementary full skyrmions in condensed matter systems [20] are observed as energy minima due to the inter-skyrmion interaction potential being repulsive and asymptotically dipolar (described in Supplementary Information and Figs. **S2** & **S3**), preventing two skyrmions to form a single composite object. The repulsive force between a pair of interacting LC skyrmions is shown in Fig. 2**b**. Through this repulsive interaction in a target skyrmion, the central skyrmion contracts due to the accumulative pressure from each exterior skyrmion ring (i.e. concentric π twist), resulting in its poor stability (Supplementary Video **S1**).

To realise stable arbitrary high-degree skyrmion configurations, we place multiple single antiskyrmions (each with degree +1) in a stretched skyrmion (the outer 'bag') *without maintaining axial symmetry*, thus forming the *skyrmion*

bags (Fig. 2**d**). These bags have a wide range of accessible topological degrees and are the first example of stable two-dimensional (2D) composite skyrmions of |degree| > 1 in monochiral materials. The range of possible distinct bag configurations echoes the plethora of nuclei described by different topological degree configurations in the original Skyrme model [9]. We denote such bag configurations of N_A antiskyrmions inside a larger bag skyrmion as $S(N_A)$, which has total topological degree $N_A - 1$. Our experimental observations of large N_A skyrmion bags indicate that they can be stable for indefinite duration, with the bags with $N_A > 1$ shown in Fig. 2 staying topologically unchanged for over one year already (contrasting with target skyrmions which disappear within seconds). Skyrmion bags interact with each other like large skyrmions (Fig. 2**c**).

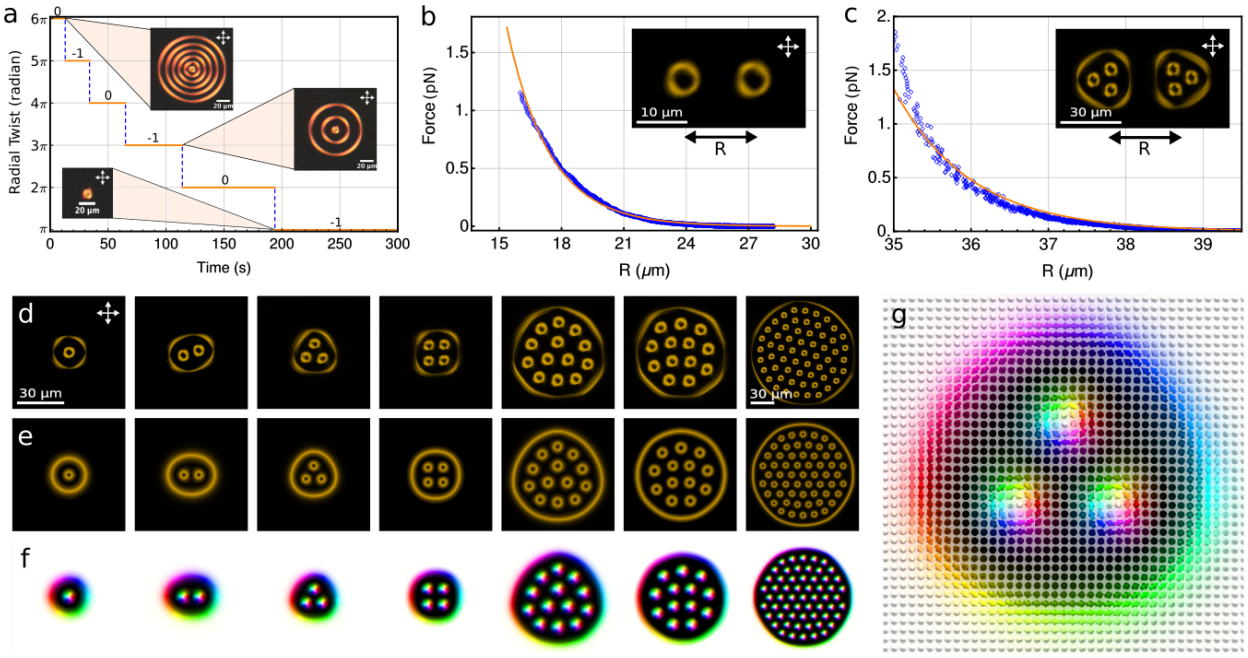

Figure 2: **Liquid crystal skyrmion bag configurations and decay of target skyrmions. (a)** A 6π-twist target skyrmion in LCs collapsing to an elementary full skyrmion within 200 seconds (video **S1**). The topological degrees (0 or -1) are labeled. **(b)** Experimental measurement of the repulsion of two LC skyrmions (points), fitted to the dipole interaction potential (Supplementary Information Eq. S2). **(c)** Experimental measurement of two repelling $S(3)$ LC bags (points), with the fitted dipole interaction potential Eq. S2 as in **(b)**. The interaction in these two cases has the same asymptotic form as between single skyrmions. **(d)** Polarising optical micrographs of skyrmion bags $S(1)$ to $S(4)$, two stable conformations of the $S(13)$ bag, and the $S(59)$ bag. The packing of antiskyrmions inside bags resembles that of hard disks–in particular, the two $S(13)$ bag configurations are analogous to the two closest packings of 13 disks [28]. **(e)** Computer-simulated counterparts of skyrmion bags in **(d)** visualized by colours based on director orientation. **(f)** Computer-simulated counterparts of skyrmion bags in **(d)** visualized by colours based on vector orientation (Fig. 1**g**). **(g)** A close-up view of a computer-simulated $S(3)$ bag visualized by coloured arrows. The experimental data were obtained with the chiral LC 5CB/cholesteryl pelargonate in **(a)** and ZLI-3412/CB-15 elsewhere.

Numerical simulations of stable skyrmion bags in LCs were performed based on minimising the Frank-Oseen free energy functional for a chiral nematic in the one-constant approximation. The energy density reads [21]

$$f = \frac{J}{2}\partial_i \boldsymbol{n} \cdot \partial_i \boldsymbol{n} + D\boldsymbol{n} \cdot (\nabla \times \boldsymbol{n}) + f_{\text{ext}}, \tag{1}$$

where J is the average elastic constant, $D = 2\pi J/p$ and p is the helical pitch of the chiral LC, and f_{ext} describes external field coupling terms and an effective uniaxial anisotropy induced by the boundary conditions of the cell. The simulated skyrmion bags are in excellent agreement with their experimental counterparts (Fig. 2 **e,f**). The topological

degrees Q of these complex configurations, as with single skyrmions, can be obtained from the integral

$$Q = \frac{1}{4\pi} \int (\boldsymbol{n} \cdot \partial_x \boldsymbol{n} \times \partial_y \boldsymbol{n})\, d^2\boldsymbol{x}. \tag{2}$$

By the convention that the arrows are oriented $(0, 0, 1)$ away from the skyrmion centre, an elementary full skyrmion has degree -1 [14]. Inside a stretched skyrmion, the arrows are oriented $(0, 0, -1)$, and an antiskyrmion placed here has degree $+1$. Hence the total degree of a $S(N_A)$ bag is $N_A - 1$ (agreeing with our configurations up to numerical precision). More complex structures have antiskyrmion bags inside skyrmion bags have been experimentally and numerically realised too (Fig. **S4**), giving a net degree $N_A - N_S$, which can in principle be any integer, positive or negative, where N_S is the total number of skyrmions and counting both N_S and N_A includes the both skyrmion and antiskyrmion bags.

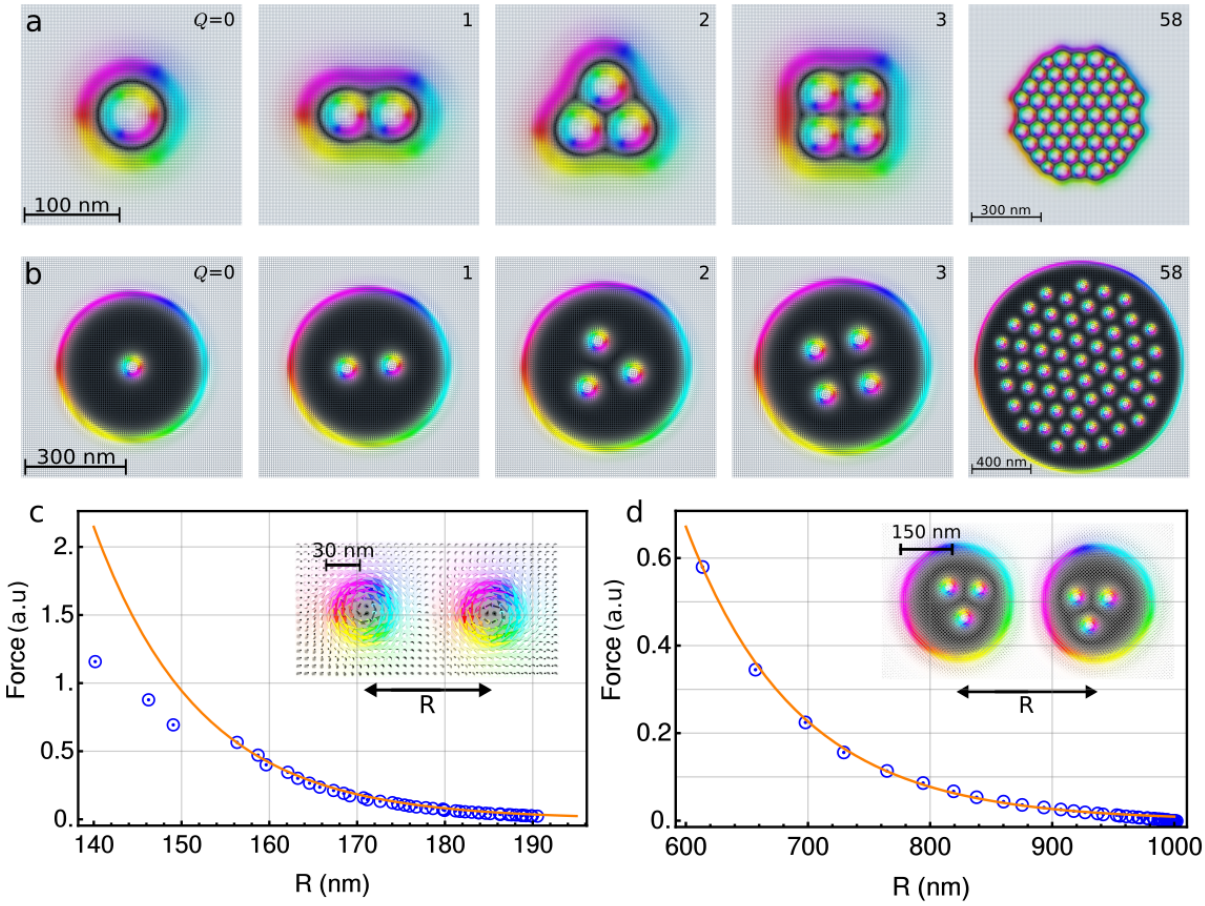

Figure 3: **Skyrmion bag configurations in chiral ferromagnets. (a)** Magnetic simulations of skyrmion bag configurations in chiral magnets with the topological degree labeled in the top-right corner of each panel. Simulations were done for $J = 7.290\ \mathrm{pJ\,m^{-1}}$, $D = 0.567\ \mathrm{mJ\,m^{-2}}$, saturation magnetisation $M_{\mathrm{sat}} = 111\ \mathrm{kA\,m^{-1}}$, corresponding to material parameters of FeGe [27], and the applied magnetic field $B = 258$ mT. **(b)** Simulations similar to those shown in **(a)**, but accounting for the demagnetising field, which were implemented using MuMax3. **(c)** Dynamical MuMax3 simulation of two magnetic skyrmions repelling (points), with the fitted dipole interaction force (Supplementary Information Eq. S2). **(d)** Dynamical MuMax3 simulation of two $S(3)$ magnetic bags repelling (points), with the fitted dipole interaction force (Eq. S2). In **(b-d)**, the physical parameters used in simulations are: $J = 20\ \mathrm{pJ\,m^{-1}}$, $D = 0.6\ \mathrm{mJ\,m^{-2}}$, $M_{\mathrm{sat}} = 900\ \mathrm{kA\,m^{-1}}$, and uniaxial anisotropy $K_u = 0.56\ \mathrm{MJ\,m^{-3}}$.

We predict 2D skyrmion bags in solid-state chiral magnets. The energy density Eq. 1 is a good description of oriented chiral materials more generally and represents a micromagnetic Hamiltonian (See Methods). We perform dynamical simulations of magnetic skyrmion bags based on the energy density in Eq. 1 and the Landau-Lifshitz-Gilbert equation using the MuMax3 finite-difference GPU accelerated code [22]. For magnetic systems, J and D

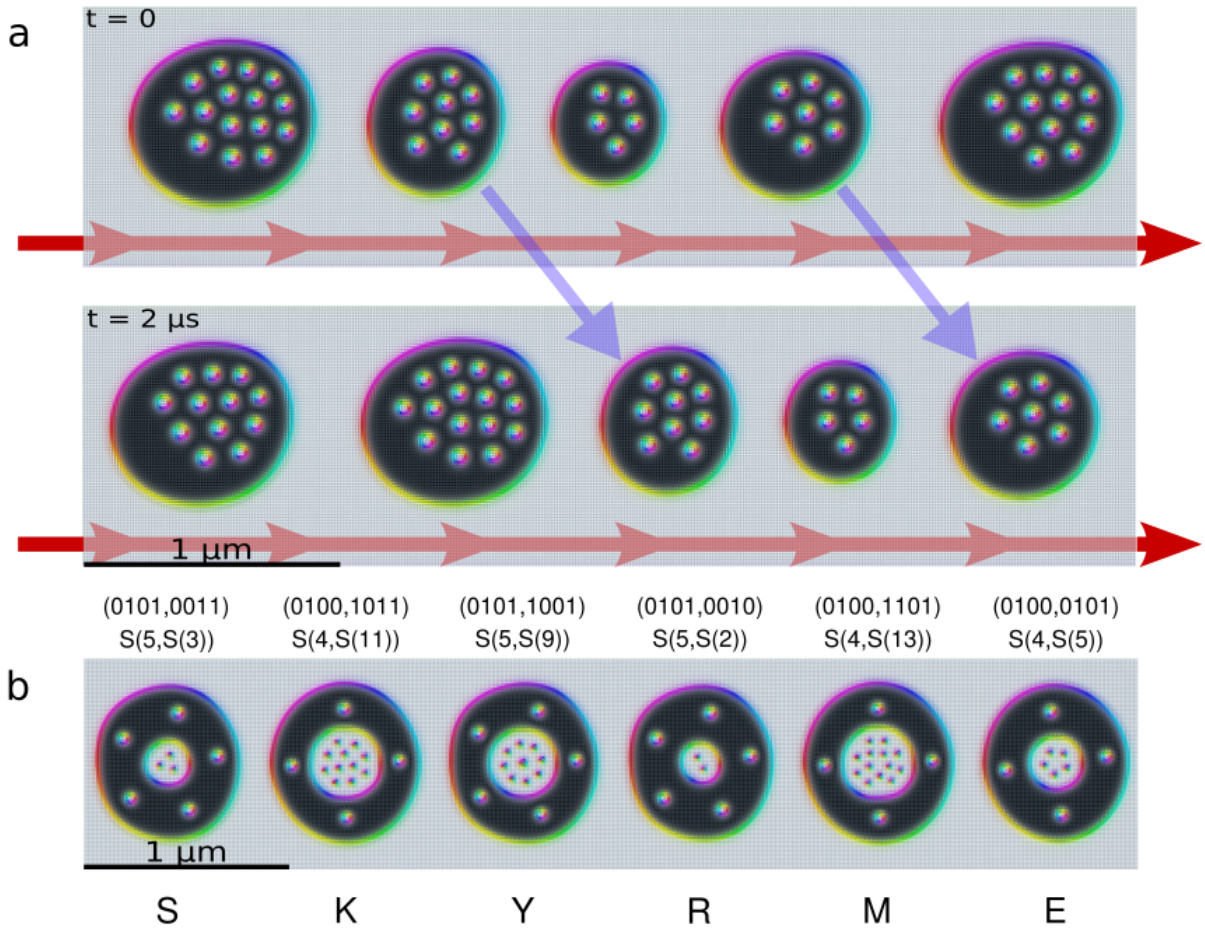

Figure 4: **Current-induced motions and data encoding of skyrmion bags. (a)** Two frames of a dynamical MuMax3 simulation of a collection of bags in a racetrack being pushed by a current. **(b)** A MuMax3 simulation of the word "SKYRME" using ASCII binary encoding of the alphabet where the outer bag holds the first four bits and the inner bag the next four bits and each full recursive bag represents a single letter and hence 8 bits of information. The simulations were made using the same parameters as those for Figure 3 **(b-d)**.

describe the exchange and Dzyaloshinskii-Moriya interaction (DMI) [23–26], where f_{ext} incorporates Zeeman coupling, magnetostatic energy, and magnetocrystalline anisotropy terms. The skyrmion bags in chiral magnets can be stabilized by an applied magnetic field (Fig.3**a**), which leads to the conformational difference compared to their LC counterparts, albeit with identical topology. The effect of including the magnetostatic energy is illustrated in Fig. 3**b**, where the demagnetising field acts as an easy-plane anisotropy, effectively expanding the outer bag skyrmion away from the inner antiskyrmions. To assess the potential effects of magnetostatic energy on stability of skyrmion bags, we have used experimental parameters of FeGe (Fig. 3**a**) [27], as well as a broad range of saturation magnetisation and uniaxial anisotropy values (Fig. 3**b**). The pair interaction of skyrmions and skyrmion bags including the nonlocal magnetostatic effect also shows a dipolar-like dependence at large separations, as shown in Fig. 3 **c,d**. Our findings show that magnetostatic energy tends to further enhance skyrmion bag stability, effectively relieving the tension exerted by the bags on the skyrmions within them.

The enhanced stability of skyrmion bags, especially at large N_A, can be understood by counting the number of nearest neighbours of each internal antiskyrmion in an optimal packing configuration, much like the mathematical circle packing problem [28] and the packing of magnetic skyrmions in nano discs [29], although in the latter case the outer radius is fixed, constraining the number of interior (anti)skyrmions. In the relaxed state, the radius of

the $S(N_A)$ bag grows with N_A. At large N_A, the number of nearest neighbour bonds in a hexagonal packing grows to 3 per skyrmion away from the edges. The energy required to push any two skyrmions together in an equilateral triangle of nearest neighbours is larger than the energy required to push together two skyrmions. Hence the bags become more stable against decay as N_A increases. Stability is further enhanced by the topology of the antiskyrmion texture. To eliminate such skyrmions within the bag, one needs to nucleate Bloch point defects, which then can eliminate the 2D skyrmions while propagating along their length [30]. The enhanced stability of skyrmion bags with large degrees is also consistent with the fact that the inter-skyrmion spacing approaches that of the hexagonal 2D skyrmion phases in both chiral LCs and magnets (Fig. **S5**). In chiral LCs, a natural inter-skyrmion distance emerges in the 2D hexagonal skyrmion lattice upon thermal quenching from the isotropic phase. This is also the case in chiral ferromagnets, where the hexagonal skyrmion A phase is the ground state in certain parameter regions, and the lattice constant is approximately the helical wavelength [23]. Therefore, the inter-skyrmion distance serves as a good measure of stability in skyrmion bags.

Magnetic skyrmion bags have potential in racetrack memory applications. Conventional proposals for racetrack memory involve encoding bits by separations between elementary full skyrmions, which is of limited density due to their repulsive interactions. Devices encoding data using the topological degree of skyrmion bags do not have this problem. For example, a train of skyrmion bags, $S(N_1), S(N_2), \ldots$, encode information by the integer N_j, the number of (anti)skyrmions in each bag. Moreover, these bags can be driven along the racetrack by a current. Figure 4**(a)** shows the micromagnetic simulation of skyrmion bags being driven by a pulsed current along a race track. The average speed of the current-driven skyrmion bags reaches ~ 1m/s at a current density 10^{10} A m^{-2} and a duty cycle 20%. There are a variety of ways skyrmion bag configurations can be utilised to store data, including nested bag configurations. For instance, nested double skyrmion bags storing 1 byte of data, by containing 1 to 16 skyrmions in one compartment, is shown in Fig. 4**(b)** to encode the word 'SKYRME' (see also Figs. **S4** & **S6**).

Our experiments and simulations have demonstrated that skyrmion bags are stable, high-degree topological configurations which occur in soft matter and magnetic systems with a range of parameters. In this sense, skyrmion bags play a role for chiral materials echoing the diversity of topological structures used to model atomic nuclei with different baryon numbers. The inventory of multiply-nested bags, however, is clearly broader than their integer topological degrees, suggesting the possibility of ultra-high density information storage.

METHODS

A. Liquid crystal experiments and simulations

1. *Materials and sample preparation.*

To assure accessibility and a broad impact of our work, pentylcyanobiphenyl (5CB, from EM chemicals) and a low-birefringence nematic mixture ZLI-3412 (EM Chemicals), commonly used and commercially available nematic LC materials, were doped with small amounts of chiral additives, cholesterol pelargonate (Sigma-Aldrich) or CB-15 (EM Chemicals), resulting in left-handed or right-handed chiral nematic LCs. The material parameters of 5CB and ZLI-3412 are listed in Table I. The helicoidal pitch p of the LC mixture is determined by $p = (\xi \cdot c)^{-1}$ where c is the weight fraction of the additive and ξ is the helical twisting power of the additive. Confining glass substrates were treated with polyimide SE1211 (Nissan Chemicals) to ensure vertical alignment of LCs at the LC-glass interface. Polyimide was applied to substrates by spin-coating at 2700 rpm for 30 s and then baked for 5 min at 90°C and then 1 h at 180°C. LC cells with gap thickness of $d = 10 - 20\mu$m were produced by sandwiching glass fibre segments in UV-curable glue. In cells where $d/p \approx 1$, spontaneous and controllably generated structures corresponding to minima of free energy were generated and manipulated using laser tweezers, as detailed below.

2. *Optical generation and repulsive force measurement of skyrmions and skyrmion bags.*

Holographic laser tweezers capable of producing arbitrary patterns of laser light intensity within the LC sample based on an Ytterbium-doped fibre laser (YLR-10-1064, IPG Photonics, operating at 1064 nm) and a phase-only spatial light modulator (P512-1064, Boulder Nonlinear Systems) integrated on an inverted microscope (IX81, Olympus) enabled generation of skyrmions and skyrmion bags and subsequent manipulations [5]. Polarising optical microscopy and video microscopy observations of LC skyrmions was done with a charge coupled device camera (Grasshopper, PointGrey Research) [5].

The experimental measurement of the repulsion of two LC skyrmions were done by producing a configuration of two LC skyrmions with a small separation. We then periodically photographed the evolution of the two-skyrmion configuration. This was then used to evaluate the rate of change of skyrmion separation, which was fitted to the highly damped equation of motion to obtain the interaction force between skyrmions $F_{\rm int} = \xi dR/dt$, where R is the skyrmion separation and ξ is the viscous drag coefficient determined from analysing Brownian motion of skyrmions [21]. Fitting experimental data with this theoretical result shows a good agreement of the model and experiments (Fig. 2**b**). The same was done with the $S(3)$ bags (Fig. 2**c**).

*3. **Numerical Simulations of LC skyrmion bags.***

For chiral LCs, the Frank-Oseen free energy density describing the energetic cost of spatial deformations of $\boldsymbol{n}(\boldsymbol{x})$ reads,

$$f = \frac{K_{11}}{2}(\nabla \cdot \boldsymbol{n})^2 + \frac{K_{22}}{2}(\boldsymbol{n} \cdot (\nabla \times \boldsymbol{n}))^2 + \frac{K_{33}}{2}(\boldsymbol{n} \times (\nabla \times \boldsymbol{n}))^2 + q_0 K_{22} \boldsymbol{n} \cdot (\nabla \times \boldsymbol{n}) + f_{\rm ext}, \tag{3}$$

where K_{11}, K_{22} and K_{33} are the splay, twist and bend elastic constants, respectively, and $q_0 = \frac{2\pi}{p}$ is the helical wavenumber. By adopting the one-constant approximation (where the bend, twist and splay elastic constants are set equal), Eq. 3 can be rewritten as Eq. 1, where $J = (K_{11} + K_{22} + K_{33})/3$ and $D = Jq_0$. The external terms

$$f_{\rm ext} = -\frac{\epsilon_0 \Delta\epsilon}{2}(\boldsymbol{n} \cdot \boldsymbol{E})^2 - \frac{\Delta\chi}{2}(\boldsymbol{n} \cdot \boldsymbol{B})^2 - W(\boldsymbol{n} \cdot \boldsymbol{n}_0)^2, \tag{4}$$

where $\Delta\epsilon$ and $\Delta\chi$ are dielectric and diamagnetic anisotropy of the LC, ϵ_0 is the vacuum permittivity, and $\boldsymbol{E}$ and $\boldsymbol{B}$ are the external electric field and magnetic field, respectively. The last term describes an effective anisotropy due to the surface anchoring on the substrates, where W is the anisotropy anchoring constant and $\boldsymbol{n}_0$ is the easy-axis direction, here coinciding with the far-field LC director. For 2D systems, these external terms can be represented by an effective anisotropy energy term $-\Lambda(\boldsymbol{n} \cdot \boldsymbol{n}_0)^2$ and $\Lambda = 4.2\mathrm{Jm}^{-3}$ was utilized in this work. Starting from initial conditions topologically equivalent to the final skyrmion bag configurations, the energy functional as the integral of Eq. 1 in a 2D plane is minimised until an energy minimum and a stable configuration is found. Details of numerical modeling are described elsewhere [31].

Material/property	K_{11} (pN)	K_{22} (pN)	K_{33} (pN)	J (pN)	D (μN m^{-1})	ξ of CB-15 (μm^{-1})	ξ of cholesterol pelargonate (μm^{-1})
5CB	6.4	3	10	6.5	4.1	7.3	-6.25
ZLI-3412	14.1	6.7	15.5	12.1	7.6	6.3	-

Table I: Material parameters of nematic LCs.

B. Magnetic Model and Simulations

1. Analytic Model

We follow, for the unit magnetisation $\boldsymbol{n}(\boldsymbol{x}) = \boldsymbol{M}(\boldsymbol{x})/|\boldsymbol{M}(\boldsymbol{x})|$, the magnetic skyrmion model of [23] using the energy density Eq. 1, where in this case the external energy is the Zeeman coupling to the external magnetic field. In this simple analytical model, demagnetising effects are not included. In Supplementary Information, the hedgehog ansatz is applied to configurations satisfying this energy functional (or, equivalently, the LC in the one-constant approximation) to find the profile of a single skyrmion, and their pairwise interaction.

2. Micromagnetic simulations

Throughout we performed magnetic simulations using the GPU-accelerated micromagnetic simulation program MuMax3 [22] with Landau-Lifshitz dynamics in the form

$$\frac{\partial \boldsymbol{n}}{\partial t} = \hat{\gamma}\frac{1}{1+\alpha^2}\left(\boldsymbol{n} \times \boldsymbol{B}_{\rm eff} + \alpha \boldsymbol{n} \times (\boldsymbol{n} \times \boldsymbol{B}_{\rm eff})\right), \tag{5}$$

where $\hat{\gamma}$ is the gyromagnetic ratio, α the dimensionless damping parameter, $\boldsymbol{B}_{\text{eff}}$ the effective field and $\boldsymbol{n}$ the magnetisation unit vector. The simulations were performed with free boundary conditions. The effective field energy derived from Eq. 1 includes contributions from exchange, anisotropy, DMI and applied field terms. Specifically, $f_{\text{ext}} = -M_{\text{sat}}\boldsymbol{B}\cdot\boldsymbol{n} - \frac{1}{2}M_{\text{sat}}\boldsymbol{B}_{\text{d}}\cdot\boldsymbol{n} - K_u(\boldsymbol{n}\cdot\boldsymbol{n}_0)^2$, where M_{sat} is the saturation magnetisation, $\boldsymbol{B}$ is an external magnetic field normal to the sample plane, $\boldsymbol{B}_{\text{d}}$ is the demagnetising field, K_u is the uniaxial anisotropy constant and $\boldsymbol{n}_0$ is the easy-axis direction, similar to the far-field orientation.

The simulation geometry is typically a 1024×1024 nm^2 square of 1 nm thickness with a cell size of $2 \times 2\times$ 1 nm^3 although for finer detail cell sizes of 1 nm^3 were used. Among other, material parameters of MnSi and FeGe [27, 32] (Supplementary Information, Table S1), common chiral magnets were used and stable structures topologically similar to the ones in LCs were obtained. To further explore the effects of magnetostatic energy (unique for magnets) on skyrmion bag stability, we probed stability of skyrmions for parameters at which these effects are most strongly pronounced. Relatively large values of saturation magnetisation were deliberately chosen to explore the effect of the magnetostatic energy, which does not destabilize the configurations even with the exaggerated values chosen here (Fig. 3**b**). Bags were simulated with bulk DMI in order that LC and micromagnetic models aligned. The material parameters used are included in the figure captions of the simulation results.

In order to probe interactions, in magnetic simulations, using Mumax3 we numerically approximated a configuration of two relaxed single skyrmions. This configuration was then dynamically evolved and the skyrmions' positions (defined as where the field $\boldsymbol{n} = (0, 0, -1)$) were tracked as a function of time. A similar procedure was performed for the bags, using the centre of the outer bag as the position. The force between skyrmions or skyrmion bags is derived from the rate of change of their absolute separation, using Thiele's equation [33].

We simulate current induced motion of skyrmion bags through the MuMax3 implementation of Zhang-Li spin-transfer torque with a current in-plane injection geometry through the racetrack [32, 34, 35]. A current density of $\sim 10^{10}\,\text{A}\,\text{m}^{-2}$ leads to a current-induced motion of the skyrmion bags along $+x$. The damping and the non-adiabatic constant of spin-transfer torque were taken to be $\alpha = 0.5$ and $\beta = 0$. The current is spin-polarized after flowing through the uniform background magnetization direction corresponding to the far-field. The Magnus force, which is often assumed to be proportional to (anti)skyrmion topological degrees, acts on the outer skyrmion bag and inner antiskyrmions in antiparallel directions [34, 35]; this skyrmion Hall effect [36] leads the antiskyrmions to cluster in the upper part of the film ($y > 0$) and stretching the bags, as can be seen in Fig. 4. The boundaries of the film are sufficiently repulsive, in this regime, to hold the bags close to the mid line. We use a pulsing current where in each cycle the current is on for 5 ns and off for 20 ns. This allows the skyrmion bags to relax towards their equilibrium configurations during the off state and mitigates the Magnus force-induced distortion of the bags.

C. Data availability

The datasets generated during and/or analysed during the current study are available from the authors on reasonable request.

[1] Bogdanov, A. & Yablonskii, D. Thermodynamically stable "vortices" in magnetically ordered crystals. The mixed state of magnets. *Zh. Eksp. Teor. Fiz* **95**, 178–182 (1989).

[2] Cortes-Ortuno, D. et al. Thermal stability and topological protection of skyrmions in nanotracks. *Sci. Rep.* **7**, 4060 (2017).

[3] Mühlbauer, S. et al., Skyrmion lattice in a chiral magnet. *Science* **323**, 915–919 (2009).

[4] Yu, X et al. Real-space observation of a two-dimensional skyrmion crystal. *Nature* **465**, 901–904 (2010).

[5] Smalyukh, I. I., Lansac, Y., Clark, N. A. & Trivedi, R. P. Three-dimensional structure and multistable optical switching of triple-twisted particle-like excitations in anisotropic fluids. *Nature Mater.* **9**, 139–145 (2010).

[6] Ackerman, P. J., Trivedi, R. P., Senyuk, B., van de Lagemaat, J, & Smalyukh, I. I. Two-dimensional skyrmions and other solitonic structures in confinement-frustrated chiral nematics. *Phys. Rev. E* **90**, 012505 (2014).

[7] Duzgun, A. & Selinger, J. V. Comparing skyrmions and merons in chiral liquid crystals and magnets. *Phys. Rev. E* **97**, 062706 (2018).

[8] Fert, A., Reyren, N., & Cros, V. Magnetic skyrmions: advances in physics and potential applications. *Nat. Rev. Mater.* **2**, 17031 (2017).

[9] Skyrme, T. H. R. A non-linear field theory. *Proc. R. Soc. Lond. A* **260**, 127–138 (1961).

[10] Planner, J. Note about Cholesterol. *Annalen der Chemie und Pharmacie.* **118**, 25–27 (1861).

[11] Reinitzer, F. Beiträge zur Kenntniss des Cholesterins. *Monatshefte fuer Chemie.* **9**, 421–441 (1888).

[12] Hornreich, R. M. & Shtrikman, S. Field-induced hexagonal blue phases in positive and negative dielectric anisotropy systems: Phase diagrams and topological properties. *Phys. Rev. A* **41**, 1978–1989 (1990).
[13] Senyuk, B. et al. Topological Colloids. *Nature* **493**, 200–205 (2013)
[14] Yu, X. Z. et al. Transformation between meron and skyrmion topological spin textures in a chiral magnet *Nature* **564**, 95–98 (2018)
[15] Iwasaki, J., Mochizuki, M., & Nagaosa, N. Current-induced skyrmion dynamics in constricted geometries. *Nature Nanotech.* **8**, 742–747 (2013).
[16] Fert, A., Cros, V., & Sampaio, J., Skyrmions on the track. *Nature Nanotech* **8**, 152–156 (2013).
[17] Schulz, T. et al. Emergent electrodynamics of skyrmions in a chiral magnet. *Nature Phys.* **8**, 301–304 (2012).
[18] Yu, X. Z. Skyrmion flow near room temperature in an ultralow current density. *Nature Commun.* **3**, 988 (2012).
[19] Zhang, X., Ezawa, M., & Zhou, Y. Magnetic skyrmion logic gates: conversion, duplication and merging of skyrmions. *Sci. Rep.* **5**, 9400 (2015).
[20] Melcher, C. Chiral skyrmions in the plane. *Proc. R. Soc. A* **470**, 20140394 (2014).
[21] Ackerman, P. J., van de Lagemaat, J., & Smalyukh, I. I. Self-assembly and electrostriction of arrays and chains of hopfion particles in chiral liquid crystals. *Nature Commun.* **6**, 6012 (2015).
[22] Vansteenkiste, A et al. The design and verification of MuMax3. *AIP Advances* **4**, 107133 (2014).
[23] Nagaosa, N. & Tokura, Y. Topological properties and dynamics of magnetic skyrmions. *Nat. nanotech.* **8**,899–911 (2013).
[24] Dzyaloshinsky, I. A thermodynamic theory of 'weak' ferromagnetism of antiferromagnetics. *J. Phys. Chem. Solids.* **4**, 241–255 (1958).
[25] Moriya, T. Anisotropic superexchange interaction and weak ferromagnetism. *Phys. Rev.* **120**, 91–98 (1960) .
[26] Fert, A & Levy, P. M. Role of anisotropic exchange interactions in determining the properties of spin-glasses. *Phys. Rev. Lett* **44**, 1538–1541 (1980).
[27] Takagi, R. et al. Spin-wave spectroscopy of the Dzyaloshinskii-Moriya interaction in room-temperature chiral magnets hosting skyrmions. *Phys. Rev. B* **95**, 220406(R) (2017)
[28] Fodor, F. The densest packing of 13 congruent circles in a circle. *Cont. Algebra and Geom.* 431–440 (2003).
[29] Zhao, X. et al. Direct imaging of magnetic field-driven transitions of skyrmion cluster states in FeGe nanodisks. *Proc. Natl. Acad. Sci. U.S.A.* **113**, 4918–4923 (2016).
[30] Milde, P. et al. Unwinding of a Skyrmion Lattice by Magnetic Monopoles. *Science* **340**, 1076–1080 (2013).
[31] Tai, J.-S. B., Ackerman, P. J., & Smalyukh, I. I. Topological transformations of Hopf solitons in chiral ferromagnets and liquid crystals *Proc. Natl. Acad. Sci. U.S.A.* **115**, 921–926 (2018).
[32] Tomasello, R., Martinez, E., Zivieri, R., Torres, L., Carpentieri, M. A strategy for the design of skyrmion racetrack memories. & Finocchio, G. *Sci. Rep.* **4**, 6784 (2014)
[33] Koshibae, W. and Nagaosa, N. Theory of skyrmions in bilayer systems. *Sci. Rep.* **7**, 42645 (2017).
[34] Fook, H. T., Gan, W. L., Lew, W. S. Gateable Skyrmion Transport via Field-induced Potential Barrier Modulation *Sci. Rep.* **6**, 21099 (2016).
[35] Iwasaki, J., Mochizuki, M., and Nagaosa, N., Universal current-velocity relation of skyrmion motion in chiral magnets, *Nature Communications* **4**, 1463 (2013)
[36] Jiang, W., et al. Direct observation of the skyrmion Hall effect. *Nature Physics* **13**, 162–169 (2017).

Acknowledgements

D.F. and M.R.D. acknowledge the fund by the Leverhulme Trust Research Programme Grant RP2013-K-009, SPOCK: Scientific Properties Of Complex Knots. Authors also thank A. Bogdanov, M. Gradhand, A. Leonov, A. Saxena, P. M. Sutcliffe and W. Zakrzewski for comments. Research at CU-Boulder (P.J.A., J.-S.B.T. and I.I.S.) was supported by the U.S. Department of Energy, Office of Basic Energy Sciences, Division of Materials Sciences and Engineering, under Award ER46921, contract DE-SC0010305.

Author contributions

C.K. originally discovered the skyrmion bag configurations. D.F. performed the theoretical analysis, with input from C.K. and M.R.D. P.J.A. and J.-S.B.T. performed the experiments with suggestions from I.I.S. and D.F. J.-S.B.T. performed the numerical analysis in LCs and C.K. in magnets. I.I.S. provided experimental techniques and materials and directed the LC component of the project. P.J.A., J.-S.B.T. and I.I.S. analysed the experimental data. All authors contributed to the preparation of the manuscript.